Wiley Online Library
Early View publication on www.wileyonlinelibrary.com
(issue and page numbers not yet assigned;
citable using Digital Object Identifier – **DOI**)

Phys. Status Solidi A, 1700124 (2017) / **DOI** 10.1002/pssa.201700124

physica status solidi a
www.pss-a.com
applications and materials science

Defect related radiative recombination in mono-like crystalline silicon wafers

E. Olsen*[,1], S. Bergan[1], T. Mehl[1], I. Burud[1], K. E. Ekstrøm[2], and M. Di Sabatino[2]

[1] Norwegian University of Life Sciences (NMBU), Universitetstunet 3, 1430 Ås, Norway
[2] Norwegian University of Science and Technology (NTNU), Alfred Getz vei 2B, 7491 Trondheim, Norway

Received 3 March 2017, revised 10 April 2017, accepted 10 April 2017
Published online 28 April 2017

Keywords defects, photoluminescence, radiative recombination, silicon, wafers

* Corresponding author: e-mail espen.olsen@nmbu.no, Phone: +47 67 23 15 66, Fax: +47 67 23 15 01

We report on studies of sub-bandgap defect related photoluminescence (DRL) signals originating from radiative recombination through traps in the bandgap of cooled mono-like silicon wafers. Spectrally resolved photoluminescence (SPL) and multivariate curve resolution (MCR) have been used in combination, to study the behaviour of sub-bandgap photoluminescence (PL) emissions in wafers cut from different heights in a pilot-scale mono-like silicon ingot. No DRL signals were found in the main mono-like body. Strong defect related sub-bandgap emissions correlating with heavily dislocated areas, are found directly above some of the seed junctions. The DRL signal exhibits a correlation with the number of axis with small angle misalignment in the junctions of the seeds. The signal conventionally labelled D1 (0.80 eV) decreases with ingot height. A mechanism relating this signal to oxygen is proposed. The signals D3 (0.94 eV) and D4 (1.00 eV) are found to co-occur, supporting previous studies, and similarly to the D2 (0.87 eV) signal, their strength is found to increase with ingot height. As the content of the transition metal impurities in the ingot is supposed to increase with height, this supports a reported link between the D3 and D4 signals with Fe, as well as a link between D2 and other impurities. An emission previously found in multicrystalline material and labelled D07 (0.70 eV), is found to solely exist as the only DRL signal recorded by us in parasitic crystals, growing into the main mono-like ingot from the crucible walls. This contradicts the common notion that the D1–D4 signals are strongly related to, and always follow dislocations.

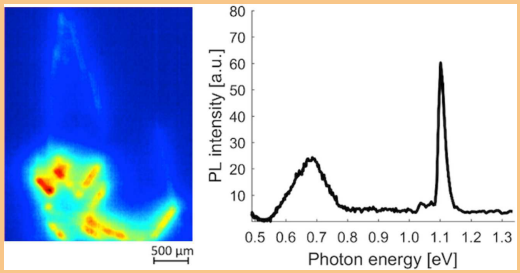

Total photoluminescence spectrum (right) and distribution (left) of the PL signal with centre energy 0.70 eV emanating from the parasitic crystals growing into the bulk mono-like Si crystal from the crucible walls.

1 Introduction Recent progress in material development for crystalline silicon solar cells has been centred around two main routes: i) high-performance multicrystalline material (HPMC) and ii) mono-like silicon. The former contains a relatively fine grain structure and a high fraction of randomly oriented grain boundaries that make it easier for dislocations to move from the interior of the grains to the boundaries, and there either interlock in the photovoltaic inactive areas or annihilate, effectively rendering them inactive with regards to recombination mechanisms [1–3]. In the latter case, measures are taken to solidify the ingot as a near-monocrystal by the relatively inexpensive directional solidification method in quartz crucibles, originally developed for making multicrystalline material [4, 5]. Both methods currently rely on seeds with the desired structure being positioned on the bottom of the crucible, with polycrystalline feedstock being positioned above before melting. The melting process has to be closely monitored in order to prevent complete melting of the respective seed structure. For HPMC fine grained seeds are preferred, while for mono-like material, the seeds at the bottom are of the monocrystalline type. Careful control of the crystal orientation of the seeds enables a monocrystalline solidification front to be established, and an essentially

monocrystalline structure to solidify towards the top. Dislocations and impurities are considered to be the main contributors to low-lifetime areas, where photogenerated charge carriers recombine causing losses in solar cell performance. Dislocations also cause breaks in the periodic crystal lattice where impurities may accumulate due to energetically favoured mechanisms. Grain boundaries with random orientation have been found to act as sinks with possible internal gettering for impurities such as iron, while Fe is found to only segregate slightly on coincidence site lattice (CSL) boundaries [6]. In mono-like silicon, dislocations readily form due to the lack of control over thermal and mechanical stresses, and due to the near-monocrystalline structure, they are relatively free to move and multiply in the ingot [7]. It has been shown that larger inclusions of SiO_2 form inside CSL grain boundaries in slowly solidified mono-like material leading to increased generation of dislocations around these as compared to a more rapidly grown material [8]. Sub-band gap DRL is caused by radiative recombination via states or traps in the bandgap by the Shockley–Read–Hall mechanism, introduced by loss in the long range periodicity of the crystal [9]. Different impurity elements and types of dislocations are known to give rise to their own characteristic states in the bandgap [10]. By cooling the wafer, phonons are removed from the structure and, due to energy conservation, more and more of recombination mechanisms involving traps become radiative – emitting photons with characteristic energies, as the temperature is lowered. In this work, we utilise a spectrally resolved photoluminescence (SPL) method of cooled mono-like wafers, to study the distribution of these mechanisms in the bottom, middle and top of a pilot-scale mono-like silicon ingot. This method has previously been employed with success for multicrystalline material [11–14]. The purpose is to study the lateral and spectral distribution of these mechanisms in order to gain fundamental insight into the distribution of impurities – possibly in combination with dislocations.

Defect related luminescence in silicon has been studied since the 1960s [15]. In 1976, a landmark article was published, in which, 4 clearly identifiable sub-bandgap signals were found to be emitted from intentionally dislocated Czochralski (Cz) monocrystalline wafers [9]. These were labelled D1–D4 (D1: 0.80 eV, D2: 0.87 eV, D3: 0.94 eV, D4: 1.00 eV) by the authors, where D indicates that they are related to dislocations, as these signals were only found in dislocated areas. More recently, several studies have been published on the topic [16–19]. The main reasons for the increased interest has mainly been related to the connection between crystal imperfections and increased recombination of minority charge carriers – both from the electronics industry perspective and from loss in silicon solar cell performance. The D1 emission is present at room temperature and has been extensively studied as it is utilised in IR-diodes [17, 20]. The D-line emissions have been linked to a number of mechanisms. In general, the D3/D4 signals are reported to occur as a pair – one, possibly, as the phonon replica of the other. Most studies suggest D3/D4 to be associated with dislocations and/or combined with impurities decorating these [16, 21, 22]. The D1 and D2 emissions are reported by some to occur together [21], while several studies find these as separate entities [13, 23]. Screw dislocations with small twist angle have been associated with the D-lines, while edge dislocations have been suggested to lead to non-radiative recombination [24]. Since the discovery and description of the original D1–D4 lines, several others have been identified. A strong, localised emission with similar peak energy as D3 (VID3) has been studied by Fløe et al. [12]. The same paper describes two possible emissions at 0.68 and 0.74 eV. To our knowledge, no firm conclusions have yet been drawn over the nature and in particular, cause of these DRL emissions. If this could be established, it could provide a valuable tool for understanding how recombination through traps in silicon is related to structure, and how defects and impurities cause areas of low lifetime of charge carriers. For the photovoltaic (PV) industry, knowing the actual distribution of individual kinds of dislocations and impurities may enable individual treatment of wafers to diminish the detrimental effects upon final solar cell performance.

2 Experimental A p-type ($10^{16}\,cm^{-3}$, B-doped), G1 (12 kg), mono-like, silicon ingot was produced in a Crystalox DS 250 pilot-scale furnace, by using 6 Cz monocrystalline seeds as reported by Ekstrøm et al. [7]. The seeds were oriented so that the crystallographic orientation of the seeds had the <110> direction parallel to the solidification direction. The seeds were deliberately positioned with respect to each other to form six inter-seed junctions with [110]/[110] boundary planes and three with [100]/[100] boundary planes. Two of the former junctions had intentionally made gaps of 0.4 and 1.6 mm. For the other junctions, the seeds were positioned in close contact. A schematic layout of the seed arrangement is shown in Fig. 1.

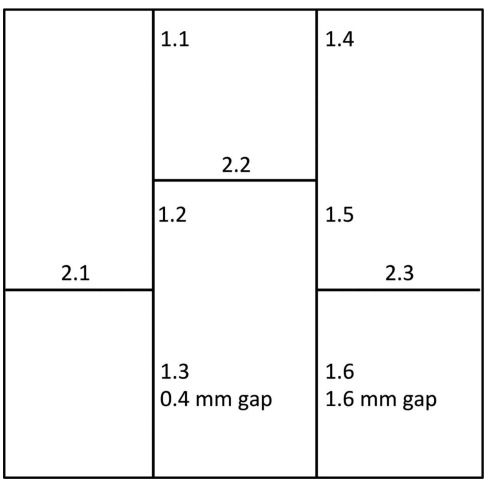

Figure 1 The layout of the initial <110> Cz monocrystalline seeds. Junctions 1.1–1.6: [110]/[110] boundary planes. Junction 2.1–2.3: [100]/[100] boundary planes. Junction 1.3 was made with 0.4 mm gap. Junction 1.6 exhibited a 1.6 mm gap.

The junctions have been numbered 1.1–1.6 ([110]/[110] boundary planes) and 2.1–2.3 ([100]/[100] boundary planes).

A thorough study of the ingot structure and development of dislocations from bottom to top, based on microscopical methods and conventional non-spectrally resolved PL, has been published by Ekstrøm et al. [7] Wafers of $156 \times 156\,mm^2$ were cut from the ingot by conventional methods. In this work, we have analysed 3 of these wafers labelled (position from the bottom of the block) A-108 (42.4 mm), A-78 (54.0 mm) and A-45 (66.3 mm). The as-cut wafers were positioned on an aluminium surface cooled by liquid nitrogen to 90 K, as previously reported for multicrystalline wafers [11–13]. The wafers were scanned using a hyperspectral camera (Specim HySpex SWIR) with a spectral range 900–2500 nm (1.34–0.49 eV) with a resolution of 6 nm. A line laser with a wavelength of 808 nm (1.53 eV) was used as excitation source. This wavelength has an average penetration depth of 12.5 μm in the silicon wafer. The illumination flux was $8 \cdot 10^{18}$ photons cm^{-2}. The lateral resolution can be varied in the range 75–500 μm by focusing the lens used with the camera. The hyperspectral data are recorded as the so-called hypercube, with a 2D image for each wavelength. A schematic view of the setup is shown in Fig. 2. In order to identify possible DRL emissions, the data recorded were analysed by multivariate curve resolution (MCR). This is a statistical-mathematical method for deconvolving complex signals composed of several individual emissions. The method has been used with success together with hyperspectral imaging on silicon wafers and solar cells in a number of previous studies [11–14]. The strength of the method lies in the ability to easily extract possible components of a very complex and highly dynamic signal, over a given range of spaxels (pixels with a spectral third dimension) in the hypercube. A strong MCR-signal in the score plot from an area indicates how strong the signal is relative to others in the spaxels where it is actually present. A strong signal in a few spaxels will show up as a strong signal in MCR, however, if the actual physical spectrum from a larger area is dominated by a strong emission, these individual signals will, to a large scale, be hidden in the integrated (averaged) spectrum making them difficult to identify by conventional methods. MCR detects such hidden signals and provides a way to identify smaller areas where they are strong. This applies very well to the convoluted PL spectra from solar cells or wafers, where the DRL signals may emanate from small areas containing individual defects, while being dominated by a large band-to-band (BB) signal from large areas with small amounts of defects. For a more thorough description of MCR we refer to Flø et al. [12]. As the method is based on a pure mathematical approach, it is preferable to check the validity of the results by first imaging the score plot from MCR, and then validating by checking for the identified high-intensity areas or pixels, i.e. what signals are actually present in the physical spectrum.

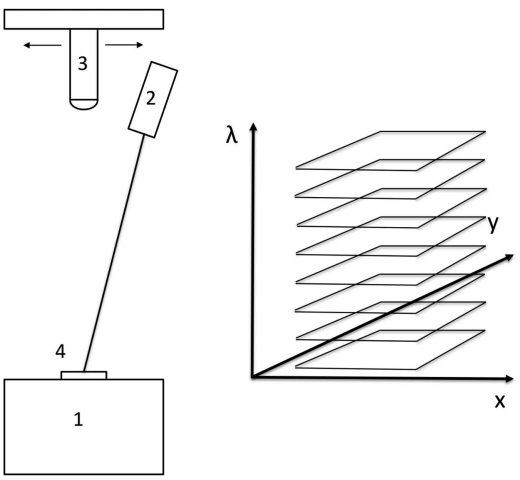

Figure 2 The hyperspectral setup (left) and a visualisation of the hypercube with one spectral- and two lateral dimensions (right). 1: Cryogenic sample holder, 2: Line laser, 3: Hyperspectral camera, 4: Sample.

3 Results and discussion

3.1 Above the seed junctions In the bottom wafer (A-108), MCR identifies three distinct components of DRL as shown in Fig. 3. Two of them correspond to D1 (0.81 eV) and D2 (0.88 eV), while the third has not been identified due to a rather low signal strength both for BB PL and DRL in this wafer. The spectra of the individual areas indicated in Fig. 3 are depicted in Figs. 4 and 5. This third signal may be a separate signal or a combination of D2 and D1. D3 (0.94 eV) and D4 (1.00 eV) are not identified by MCR as separate signals in this wafer. Physical spectra from the areas above the junctions are depicted in Fig. 6. In general, DRL from the junctions increases with ingot height, from the bottom to the top. The same signals occur in all junctions, except in 1.5 where there is no recorded DRL. Junction 2.3 clearly exhibits the strongest signal. The junctions with intentionally made gaps (1.3 and 1.6) exhibit similar DRL emission, as some junctions with no gaps, except for junction 2.3. This junction, however, exhibits a significantly larger DRL emission than the others.

In wafer A-78, cut from the middle of the ingot, the D3 (0.94 eV) and D4 (1.00 eV) signals are clearly identified by MCR integrated over the total wafer (Fig. 3), together with the three signals previously described in wafer A-108. An additional signal between D2 and D3 is also found. Judging from the physical spectra in Fig. 4, there are 4 clearly identifiable emissions (D1–D4). The emission between D2 and D3, as identified by MCR, cannot be distinguished clearly by eye from the recorded spectrum. However, as MCR constitutes a highly powerful algorithm, not being able to identify a component by eye in a complex and convolved spectrum does not constitute a verification of its absence. This will be further examined in Section 3.3 below. Junction 1.5 exhibits no DRL, while junctions 1.2 and 2.2 only exhibit a small amount. Junction 2.3, however, shows

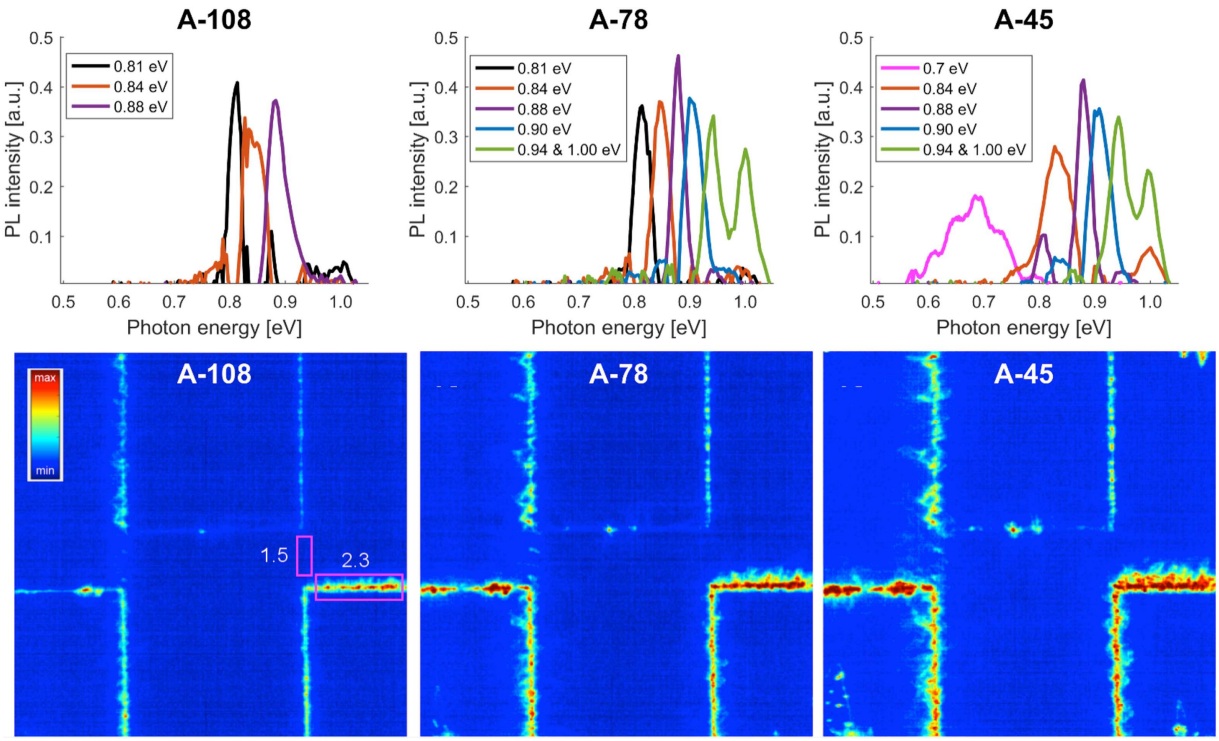

Figure 3 Image of the total DRL (BB PL, 1.1 eV omitted) signal at 90 K for the respective wafers (bottom) and the corresponding results from the MCR analysis (top). The red boxes in A-108 indicate the area for the MCR analysis.

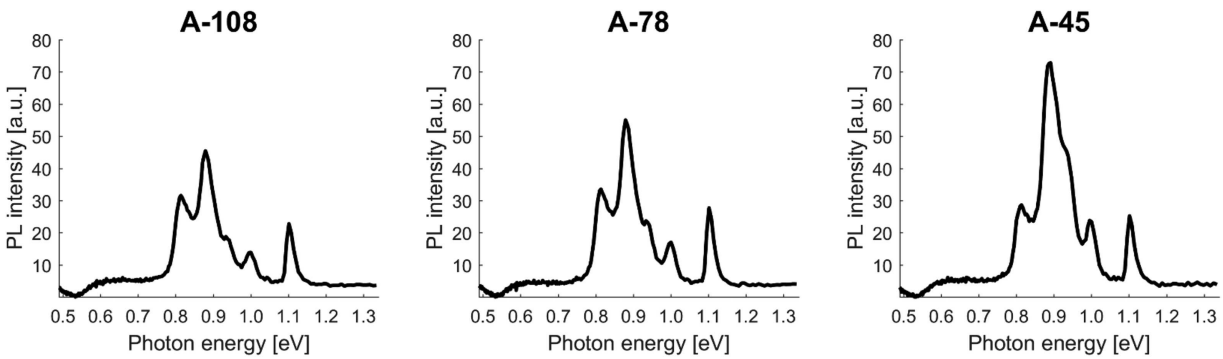

Figure 4 Total spectra (0.5–1.3 eV) from the area above junction 2.3 as indicated in Fig. 3 in the three studied wafers.

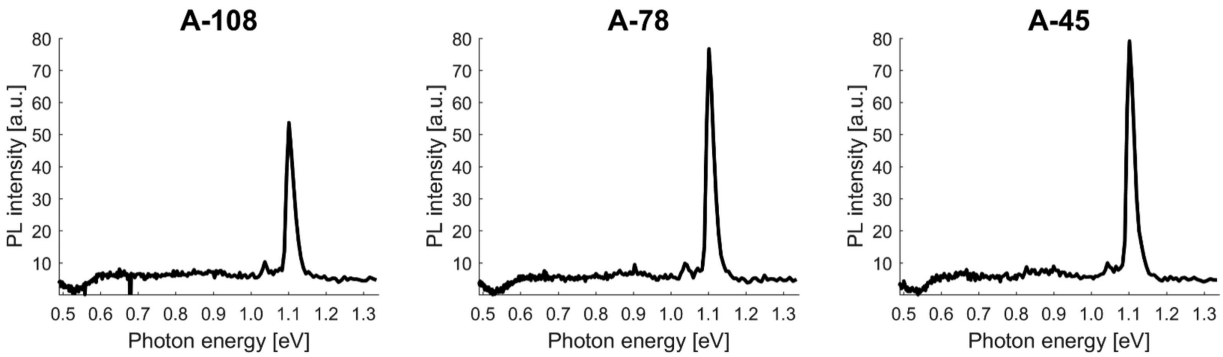

Figure 5 Total spectra (0.5–1.3 eV) from the area above junction 1.5 in the three studied wafers. No clear indications of any D-line emissions are found.

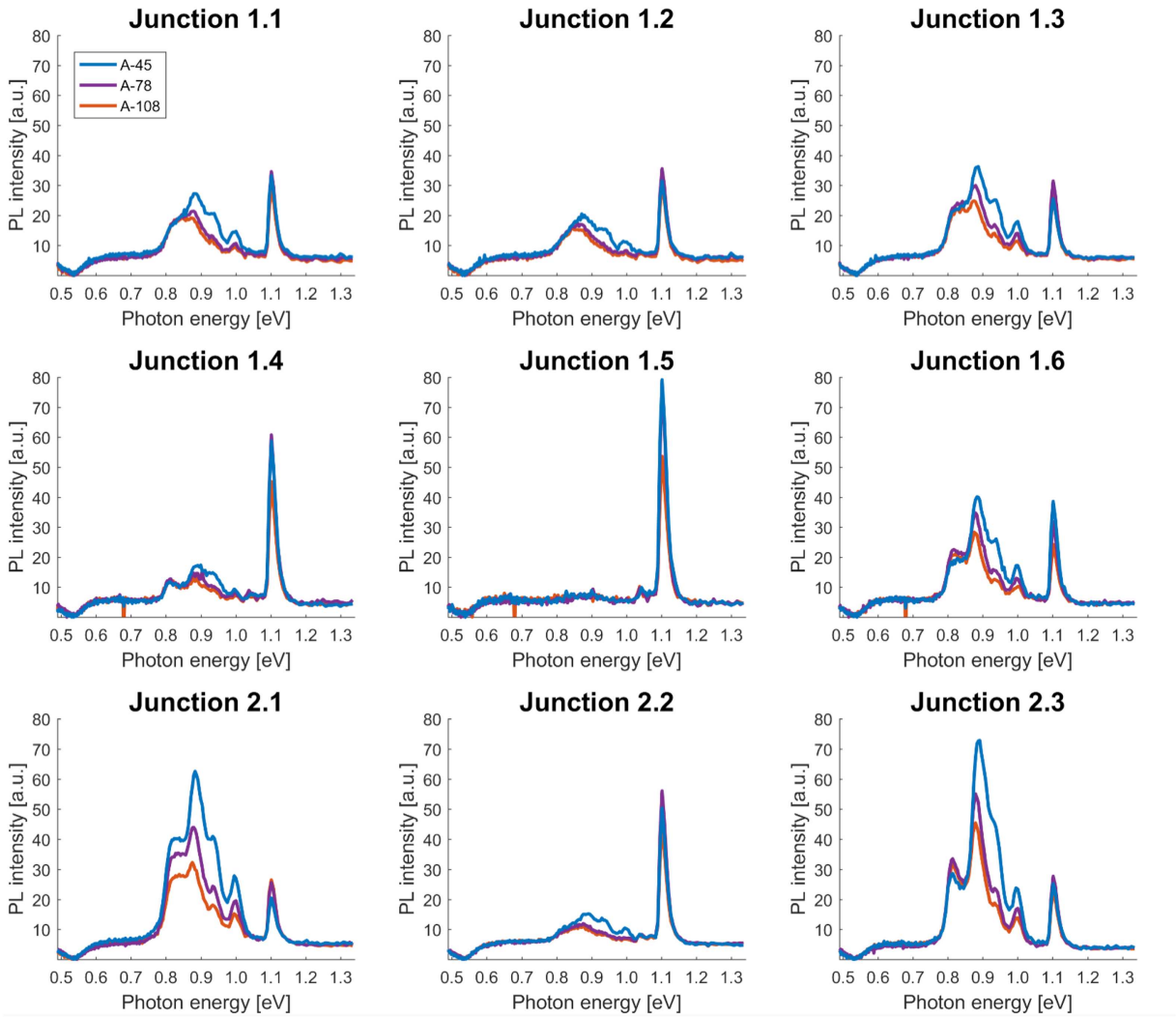

Figure 6 DRL from areas above the individual seed junctions in the wafers investigated.

strong DRL for all the emissions D1–D4. Junctions 1.3 and 1.6 do not show a significant difference with regards to DRL or BB PL.

In wafer A-45, the D1–D4 signals again occur in the MCR analysis for the whole wafer – except for the signal between D1 and D2. However, a notable new and broad signal is identified with peak energy around 0.7 eV [14]. A more thorough investigation reveals that the signal identified by MCR, with energy intermediate between D2 and D3, is a separate entity. An emission with this energy has previously been suggested in multicrystalline material, and will be given a further discussion below. Physical spectra from the junction areas again show D1–D4 with similar relative intensities in the individual junctions as for the other wafers. No significant DRL is recorded in junction 1.5, only small amounts in 2.2 and 1.2, while junction 2.3 exhibits a very strong signal. DRL shows similar strength in junctions 1.3 (0.4 mm gap) and 1.6 (1.6 mm gap).

In the work by Ekstrøm et al., the dislocation density over each junction through the ingot is identified to be a function of the number of principal axes with low-angle misorientation between the individual junctions for the seed crystals [7]. Junction 2.3 exhibits a relatively large misorientation in all three axes (x, y, z), while junction 1.5 is almost perfectly aligned. The DRL signal, as well as the BB PL signal from the area above the seed junctions, show the same pattern as the dislocation densities. The two junctions with intentionally made gaps (1.3 and 1.6), both exhibit similar DRL activities–in the intermediate range. These observations support the conclusions made by Ekstrøm et al., that dislocation formation is more a function of misorientation than of gap width.

3.2 Parasitic crystals The ingot exhibited a certain degree of breakdown of the mono-like structure, due to nucleation of parasitic crystals at the crucible wall during solidification. This led to a multicrystalline structure in the periphery of the ingot, close to the crucible walls, that continued to grow inwards, into the main mono-like bulk as solidification proceeded. When the centre $156 \times 156\,\text{mm}^2$

block was cut, most of the multicrystalline parts were cut away, however, some of it remained in the topmost wafers, particularly in the corners [7]. The MCR analysis of the integrated spectrum over the wafer A-45 identified a previously reported signal D07 in the top wafer, as seen in Fig. 3 (right) [14]. Further examination revealed this signal to be confined to the small, multicrystalline crystallites. This is evident in Fig. 7. This emission was not detected elsewhere in the ingot. Fig. 7c and d shows close-ups of two of the parasitic crystals together with the spectrum from one of the high-intensity areas (Fig. 7e).

An emission with peak energy around 0.69 eV has previously been reported for multicrystalline wafers as emanating from distinct, small, and well localized areas [14]. It is evident from Fig. 7 that this is also the case for the parasitic crystals in this mono-like ingot. However, there is a clear signal following the boundary between the mc-Si and the mono-like Si as seen in Fig. 7c and d. The latter is most probably a primary grain boundary with a width of several micrometres. Such boundaries may function as sinks for impurities such as Fe and O, forming clusters within the structure. This is thermodynamically favourable, as the energy associated with harbouring impurities is lower in these regions than in the Si crystal structure with high periodicity. No other DRL emissions are found in these parasitic crystals. This behaviour is unexpected, as these crystallites exhibit high etch pit densities, and thereby, a large number of dislocations as compared to the mono-like bulk ingot [7]. Dislocated multicrystalline material only exhibiting the D07 DRL has not been reported before, and contradicts the common notion that the D1–D4 signals follow dislocations and/or dislocations decorated with impurities. Most previous studies have been focused on the D1–D4 emission lines (0.80–1.00 eV) and a few studies have been reported for energies below 0.75 eV. The D1 line has been linked to oxygen precipitates [17, 25]. This may also be the case for the D07 (0.70 eV) signal. Being close to the top of the ingot it is expected that, in particular the multicrystalline parts, will contain significant amounts of impurities due to segregation effects. This calls for further studies of these structures. The D07 signal has previously been attributed to Fe_i [14]. The observations in this study, where the D07 signal is of localized character, rather suggest this signal to be linked to inclusions. However, a resolution of 0.75 μm cannot distinguish if the signal is following small subgrains formed in the mc-Si crystallites, as reported by Mehl et al. [26]. These studies of FeB–Fe_i in HPM wafers with high-definition PL show a very similar distribution of Fe as found in this study. According to Graff, Fe has an acceptor trap level at $E_T = E_V + 0.4$ eV, consistent with a recombination mechanism involving free electrons from the conduction band, to recombine via this level with an emitted photon energy $E_{ph} = E_C - E_T = 1.09 - 0.4\,\text{eV} = 0.69\,\text{eV}$ consistent with our findings [10]. This calls for further

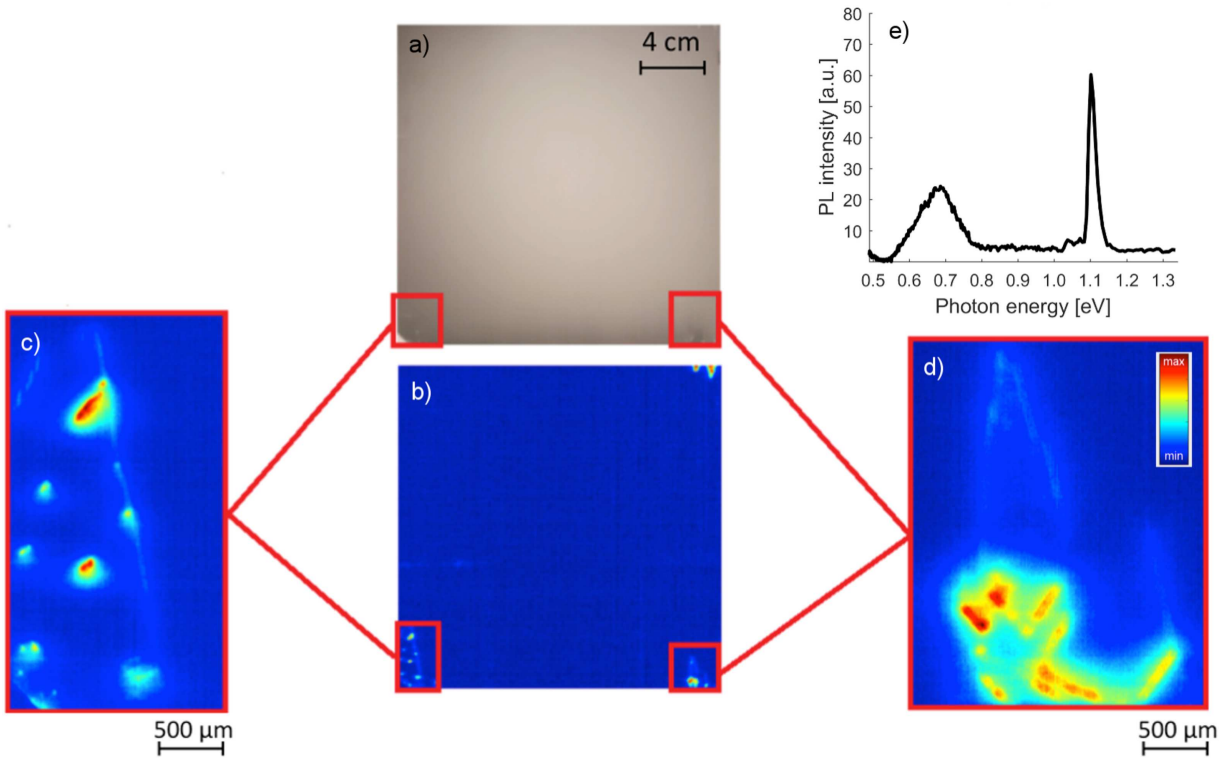

Figure 7 a) RGB image of the top wafer A-45. b) Image of the MCR score plot for the D07 (0.694 eV) emission for the whole wafer. c) and d) Close up of the MCR score plot for the D07 signal for two of the parasitic multicrystalline crystallites, pixel resolution 75 μm. e) Recorded spectrum from the area indicated in d.

studies of these structures by methods with high magnification such as TEM.

3.3 The 0.9 eV emission A DRL emission with peak energy of 0.90 eV has been identified in the convolved spectrum by MCR in wafers A-78 and A-45 (Fig. 3). Since the MCR score plot shows no DRL in the main bulk mono-like ingot, this signal must come from the areas above the seeds or the parasitic crystals. Since the parasitic crystals only exhibit the D07 emission, the signal must be related to the dislocated areas above the seed junctions. Further examinations of the recorded spectrum in individual pixels from the hyperspectral images of the junction areas revealed that this indeed is a separate DRL emission. A plot for the total recorded emission with a centre energy of 0.90 eV over the whole A-45 wafer with individual spectra for certain identified pixels is shown in Fig. 8.

As seen from Fig. 8, the 0.9 eV signal is found in DRL active areas in all junctions, except in the DRL inactive junction 1.5. An emission with a peak around 0.9 eV has been observered by Lausch et al. for a certain crystallographic defect [14]. It has further been seen in microcrystalline thin film Si and been attributed to Si–H bonds. The observation of this distinct emission in the junction areas of as-cut mono-like wafers without any treatment means that – at least in this case, it cannot be attributed to Si–H bonds.

4 Summary and conclusions The current work reports on examination of defect-related sub-bandgap photoluminescence from three wafers, cut from various heights in a mono-like ingot, with dislocated areas above the seed junctions. No DRL is found in the main, mono-like structure. The DRL from the junction areas are found to exhibit emissions consistent with previous studies of intentionally dislocated Cz wafers. The D1 emission is found to be the strongest in the bottom wafer and the weakest in the top, supporting previous suggestions that it is associated with oxygen. The D2 emission is strongest in the uppermost wafer, supporting the theories that it is associated with transition metal impurities. The D3 and D4 emissions occur as a pair and are not found in the bottom wafer, but are found in the middle- and are even stronger in the top wafer. This pair has been reported to be linked to iron or iron precipitates on dislocations. Our findings support this explanation. Further studies with complementary methods are needed to firmly establish the cause and nature of these emissions. Small areas of multicrystalline nature are found to have grown into the main, mono-like structure around the corners in the top part of the ingot. These are heavily dislocated but only exhibit one strong, broad emission with centre frequency around 0.69 eV. As dislocated areas normally exhibit all four D-band emissions – in particular high in ingots, this is a highly unexpected result which raises questions regarding the physical mechanisms and interactions between dislocations and impurities, leading to the commonly found D1–D4 emissions in silicon wafers. Studies involving splitting the FeB pair by illumination suggest the D07 emission to be caused by Fe_i [26]. We

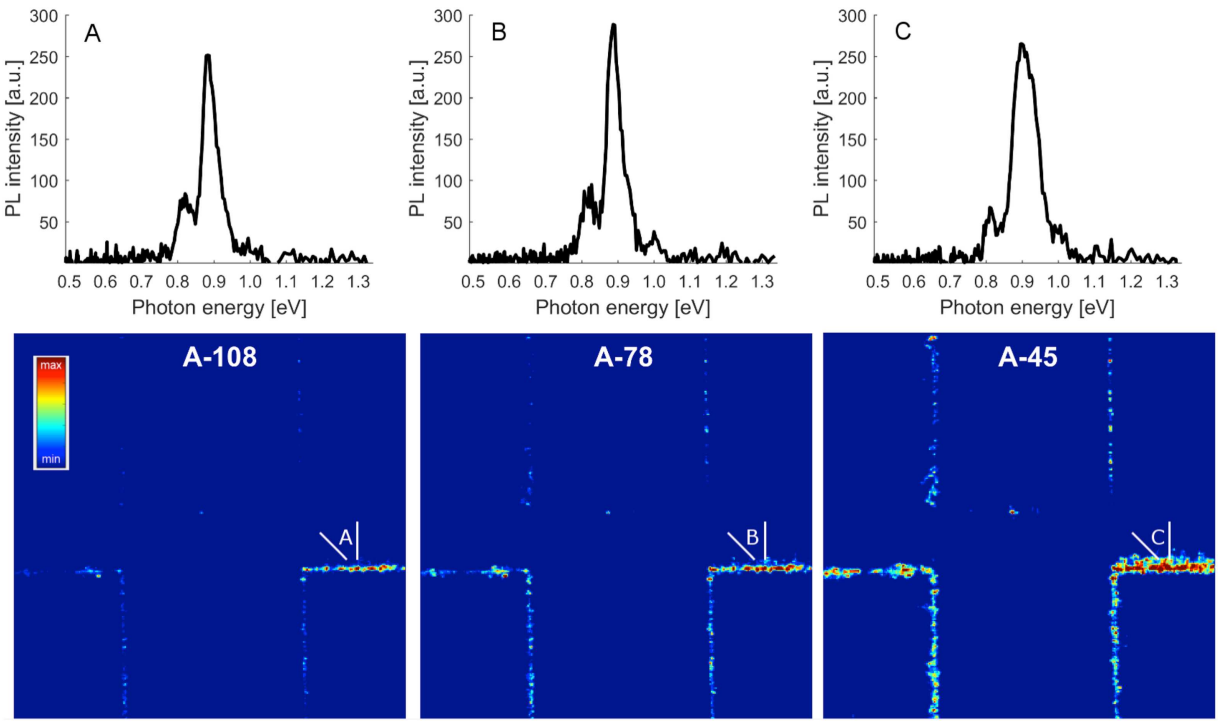

Figure 8 Recorded spectra (top) and maps (bottom) of the 0.90 eV signal in wafer A-108 (left), A-78 (middle) and A-45 (right). The spectra shows the signal in one position over junction 2.3 common to all three wafers exhibiting strong emission.

suggest this emission is caused by recombination between the conduction band edge E_C and the known trap generated by Fe at $E_T = E_V + 0.4\,eV$ [27]. An emission with peak energy of 0.90 eV has been found in the dislocated, DRL active junctions. A trap level consistent with this has been reported to be caused by Si–H bonds [28]. As our samples have not been subject to hydrogenation, this cannot be the case for this material. It is natural to put this into the same category as the other emissions related to impurities, as they will accumulate towards the top of the wafer due to segregation.

References

[1] C. W. Lan, W. C. Lan, T. F. Lee, A. Yu, Y. M. Yang, W. C. Hsu, B. Hsu, and A. Yang, J. Cryst. Growth **360**, 68 (2012).
[2] Y. M. Yang, A. Yu, B. Hsu, W. C. Hsu, A. Yang, and C. W. Lan, Prog. Photovolt. **23**, 340 (2015).
[3] S. Castellanos, K. E. Ekstrom, A. Autruffe, M. A. Jensen, A. E. Morishige, J. Hofstetter, P. Yen, B. Lai, G. Stokkan, C. del Canizo, and T. Buonassisi, IEEE J. Photovolt. **6**, 632 (2016).
[4] M. Trempa, C. Reimann, J. Friedrich, D. Muller, and Oriwol, J. Cryst. Growth **351**, 131 (2012).
[5] X. Gu, X. G. Yu, K. X. Guo, L. Chen, D. Wang, and D. R. Yang, Sol. Energy Mater. Sol. Cells **101**, 95 (2012).
[6] M. Knörlein, A. Autruffe, R. Søndena, and M. Di Sabatino, Energy Procedia **55**, 6 (2014).
[7] K. E. Ekstrøm, G. Stokkan, R. Sondena, H. Dalaker, T. Lehmann, L. Arnberg, and M. Di Sabatino, Phys. Status Solidi A **212**, 2278 (2015).
[8] A. Autruffe, M. Kivambe, L. Arnberg, and M. Di Sabatino, Phys. Status Solidi A **213**, 122 (2016).
[9] N. A. Drozdov, A. A. Patrin, and V. D. Tkachev, JETP Lett. **23**, 597 (1976).
[10] K. Graff, Metal Impurities in Silicon-Device Fabrication (Springer, Berlin, 2000).
[11] E. Olsen and A. S. Flo, Appl. Phys. Lett. **99**, 11903 (2011).
[12] A. Fløe, I. Burud, K. Kvaal, R. Sondena, and E. Olsen, AIP Adv. **3**, 112120 (2013).
[13] I. Burud, A. S. Flo, and E. Olsen, AIP Adv. **2**, 042135 (2012).
[14] D. Lausch, T. Mehl, K. Petter, A. S. Flo, I. Burud, and E. Olsen, J. Appl. Phys. **119**, 054501 (2016).
[15] P. J. Dean, J. R. Haynes, and W. F. Flood, Phys. Rev. **161**, 711 (1967).
[16] R. Sauer, J. Weber, J. Stolz, E. R. Weber, K. H. Kusters, and H. Alexander, Appl. Phys. A: Mater. **36**, 1 (1985).
[17] S. Pizzini, M. Acciarri, E. Leoni, and A. Le Donne, Phys. Status Solidi B **222**, 141 (2000).
[18] I. Tarasov, S. Ostapenko, C. Haessler, and E. U. Reisner, Mater. Sci. Eng. B **71**, 51 (2000).
[19] M. Tajima, Y. Iwata, F. Okayama, H. Toyota, H. Onodera, and T. Sekiguchi, J. Appl. Phys. **111**, 113523 (2012).
[20] V. V. Kveder, E. A. Steinman, S. A. Shevchenko, and H. G. Grimmeiss, Phys. Rev. B **51**, 10520 (1995).
[21] T. Sekiguchi and K. Sumino, J. Appl. Phys. **79**, 3253 (1996).
[22] T. Arguirov, Electro-optical properties of dislocations in silicon and their possible applications for light emitters, PhD Thesis, (Brandenburger Technische Universität Cottbus, Cottbus, 2007).
[23] S. Ostapenko, I. Tarasov, J. P. Kalejs, C. Haessler, and E. U. Reisner, Semicond. Sci. Tech. **15**, 840 (2000).
[24] T. Mchedlidze, T. Arguirov, O. Kononchuk, M. Trushin, and M. Kittler, Phys. Status Solidi C **8**, 4 (2011).
[25] S. Pizzini, M. Guzzi, E. Grilli, and G. Borionetti, J. Phys. Condens. Matter. **12**, 10131 (2000).
[26] T. Mehl, M. Di Sabatino, K. Adamczyk, I. Burud, and E. Olsen, Energy Procedia **92**, 130 (2016).
[27] A. A. Istratov, H. Hieslmair, and E. R. Weber, Appl. Phys. A **69**, 13 (1999).
[28] D. Redifield and R. Bube, Photoinduced defects in semiconductor silicon, (Cambridge University Press, Cambridge, UK, 1996).

